CHINESE OPTICS LETTERS

Vol. 19, No. 8 | August 2021

Nanoplasmonic magneto-optical isolator [Invited]

Vahid Foroughi Nezhad[1,2], Chenglong You[3], and Georgios Veronis[1,2*]

[1] School of Electrical Engineering and Computer Science, Louisiana State University, Baton Rouge, Louisiana 70803, USA

[2] Center for Computation and Technology, Louisiana State University, Baton Rouge, Louisiana 70803, USA

[3] Department of Physics and Astronomy, Louisiana State University, Baton Rouge, Louisiana 70803, USA

*Corresponding author: gveronis@lsu.edu

Received April 30, 2021 | Accepted June 20, 2021 | Posted Online July 28, 2021

We introduce a nanoplasmonic isolator that consists of a cylindrical resonator placed close to a metal-dielectric-metal (MDM) waveguide. The material filling the waveguide and resonator is a magneto-optical (MO) material, and the structure is under an externally applied static magnetic field. We theoretically investigate the properties of the structure and show that the cavity mode without MO activity splits into two modes when the MO activity is present. In addition, we find that the presence of the MDM waveguide leads to a second resonance due to the geometrical asymmetry caused by the existence of the waveguide. We also show that, when MO activity is present, the cavity becomes a traveling wave resonator. Thus, the transmission of the structure depends on the direction of the incident light, and the proposed structure operates as an optical isolator.

Keywords: plasmonics; metal optics; magneto-optic systems.

DOI: 10.3788/COL202119.083602

1. Introduction

Nonreciprocal elements such as circulators and isolators are essential for the realization of integrated optical circuits[1]. The design of nonreciprocal components requires breaking the time reversal symmetry[2,3]. This can be achieved through the use of nonlinear materials[4,5], materials with time-dependent properties[6], and magneto-optical (MO) materials[7]. However, since the MO response of natural materials is weak at optical wavelengths, designing nonreciprocal devices that are based on MO materials results in bulky structures that are much larger than the wavelength[8]. The advent of silicon photonics and photonic crystals has reduced the size of nonreciprocal optical components down to wavelength scale[9–12]. To further decrease the size down to the subwavelength scale, one needs to beat the diffraction limit. Nanoscale metallic structures that support surface plasmon polaritons can be used to achieve subwavelength scale optical components, because they can beat the diffraction limit[13,14]. Combining metallic and MO materials can therefore pave the way for highly compact nonreciprocal plasmonic elements[15–22]. One of the promising ways to engineer integrated plasmonic circuits is to employ metal-dielectric-metal (MDM) waveguides[23]. Several different nanoscale plasmonic components based on MDM waveguides have been proposed, including filters[24,25], couplers[26,27], sensors[28–30], switches[31–35], and rectifiers[36].

In this paper, we introduce a nanoplasmonic isolator, which consists of a cylindrical resonator placed close to an MDM waveguide. The material filling the waveguide and resonator is an MO material, and the structure is under an externally applied static magnetic field. We first investigate the modes of the cylindrical cavity resonator when the MDM waveguide is absent. We show that the cavity mode without MO activity splits into two modes when MO activity is present. Results for the wavelength splitting obtained with first-order perturbation theory agree well with the exact results. We then investigate the coupling between the MDM waveguide and the cavity. We find that the presence of the MDM waveguide leads to a second resonance due to the geometrical asymmetry caused by the existence of the waveguide. In the presence of both the MDM waveguide and MO activity, the mode splitting is due to both geometrical asymmetry and MO activity. We also show that, when MO activity is present, the cavity becomes a traveling wave resonator. Traveling wave modes do not decay equally into the forward and backward propagating MDM waveguide modes due to momentum matching. As a result, the transmission of the structure depends on the direction of the incident light. The proposed structure therefore operates as an optical isolator. We also find that there is a tradeoff between the isolation ratio and the insertion loss, as the geometrical parameters of the structure are varied.

2. Results

Figure 1 shows the schematic of the proposed nanoplasmonic isolator. We consider a two-dimensional structure with no field

© 2021 Chinese Optics Letters

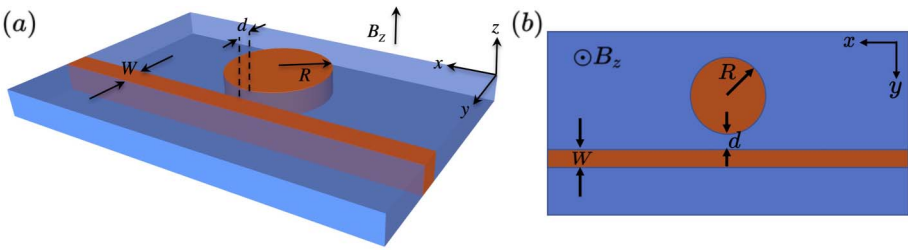

Fig. 1. (a) Nanoplasmonic isolator that consists of a cylindrical cavity with radius R placed close to an MDM waveguide with width W. The metal and MO material are shown with blue and orange colors, respectively. The structure is under a static magnetic field in the z direction. (b) Cross-sectional view of the structure at the $z = 0$ plane.

variation in the z direction. The device consists of a cylindrical resonator placed close to an MDM waveguide. The structure is under a static magnetic field in the z direction. The metal is silver. For the dielectric permittivity of silver ϵ_m, we use the Drude model with a dielectric constant at infinite frequency $\epsilon_\infty = 3.7$, bulk plasmon frequency $\omega_p = 9.1$ eV, and collision frequency $\gamma = 0.018$ eV[37]. The material filling the waveguide and resonator is an MO material. A tensor describes the dielectric permittivity of the MO material under a static magnetic field in the z direction:

$$\bar{\bar{\epsilon}} = \epsilon_0 \begin{bmatrix} \epsilon_r & i\alpha & 0 \\ -i\alpha & \epsilon_r & 0 \\ 0 & 0 & \epsilon_\perp \end{bmatrix}, \tag{1}$$

where α is the strength of MO activity. Bismuth iron garnet (BIG) is the MO material that we use here with $\epsilon_r = 6.25$ and $\alpha = 0.06$[15,38], which saturates in an externally applied static magnetic field of 150 mT[39].

2.1. Cavity modes when the MDM waveguide is absent

We first investigate the resonance condition and modes of the cylindrical cavity resonator exposed to a static magnetic field when the MDM waveguide is absent. By applying the boundary conditions at the metal-dielectric interface at $\rho = R$, one can derive the following resonance condition for the TM modes supported by the cavity[40]:

$$\frac{m\alpha}{\epsilon_r \epsilon_e R} + \frac{k_1 J_m'(k_1 R)}{\epsilon_e J_m(k_1 R)} = \frac{k_2 H_m^{(2)'}(k_2 R)}{\epsilon_m H_m^{(2)}(k_2 R)}, \tag{2}$$

where m is the azimuthal mode number, J_m is the mth-order Bessel function of the first kind, $H_m^{(2)}$ is the mth-order Hankel function of the second kind, $k_1 = k_0\sqrt{\epsilon_e}$, $k_2 = k_0\sqrt{\epsilon_m}$, and $\epsilon_e = \epsilon_r - \alpha^2/\epsilon_r$. In addition, $k_0 = \omega/c$ is the free-space wave number. In the presence of a material loss in the metal, the solutions, which satisfy Eq. (2), are complex[37]. Here, we only consider low-order modes, which have relatively low loss, so that the corresponding solutions of Eq. (2) have a small imaginary part. Each cavity mode is characterized by two mode numbers, the radial mode number n and the azimuthal mode number m. The fundamental mode of the cavity has $m = n = 1$. When the off-diagonal elements of the dielectric permittivity tensor in Eq. (1) are set equal to zero ($\alpha = 0$), Eq. (2) reduces to the resonance condition for an isotropic cylindrical resonator[37]. There are two differences between the resonance conditions for an isotropic cylindrical resonator[37] and for an anisotropic cylindrical resonator filled with an MO material [Eq. (2)]: when the resonator is filled with an MO material ($\alpha \neq 0$), the first term on the left side of Eq. (2) is nonzero. In addition, the second term on the left side of Eq. (2) is modified, since ϵ_e is different than ϵ_r for $\alpha \neq 0$. In the absence of the first term on the left side of Eq. (2), the $\pm m$ cavity modes are degenerate with the same resonant wavelength. In the presence of an MO material ($\alpha \neq 0$), the first term on the left side of Eq. (2) breaks the symmetry between the $\pm m$ cavity modes. These modes are no longer degenerate, since they have different resonant wavelengths. The cavity mode with resonant wavelength λ_c without MO activity ($\alpha = 0$) splits into two modes with resonant wavelengths $\lambda_\pm = \lambda_{cm} \pm \Delta\lambda/2$ when MO activity is present ($\alpha \neq 0$). This is analogous to the Zeeman splitting of electronic states in atoms[41,42]. We calculate by solving Eq. (2) the resonant wavelengths of the cylindrical resonator when the MDM waveguide is absent ($d = \infty$ in Fig. 1) as a function of the radius R of the cylindrical cavity in the presence and absence of MO activity [Fig. 2(a)]. As expected, increasing R increases the resonant wavelengths of the structure [Fig. 2(a)]. The dependence of the resonant wavelengths on the radius R is approximately linear. We also calculate the resonant wavelengths of the cylindrical resonator when the MDM waveguide is absent using the finite-difference-frequency-domain (FDFD) method [Fig. 2(a)]. We observe that there is excellent agreement between the results obtained by solving Eq. (2) and the numerical results obtained using the FDFD method. Since the functionality of the structure of Fig. 1 as an isolator is based on the cavity mode splitting when MO activity is present, we investigate the dependence of the wavelength splitting $\Delta\lambda$ when MO activity is present on the parameters of the structure. More specifically, we use the first-order perturbation theory and find the following expression for the wavelength splitting $\Delta\lambda$[42]:

$$\Delta\lambda \approx \frac{m\alpha\lambda_c^3 |J_m(k_1' R)|^2}{\pi^2 \epsilon_r \epsilon_e \left[\int_0^R |J_m(k_1'\rho)|^2 \rho \mathrm{d}\rho + \frac{|J_m(k_1' R)|^2}{|H_m^{(2)}(k_2 R)|^2} \int_R^\infty |H_m^{(2)}(k_2\rho)|^2 \rho \mathrm{d}\rho\right]}, \tag{3}$$

where $k_1' = 2\pi\sqrt{\epsilon_r}/\lambda_c$.

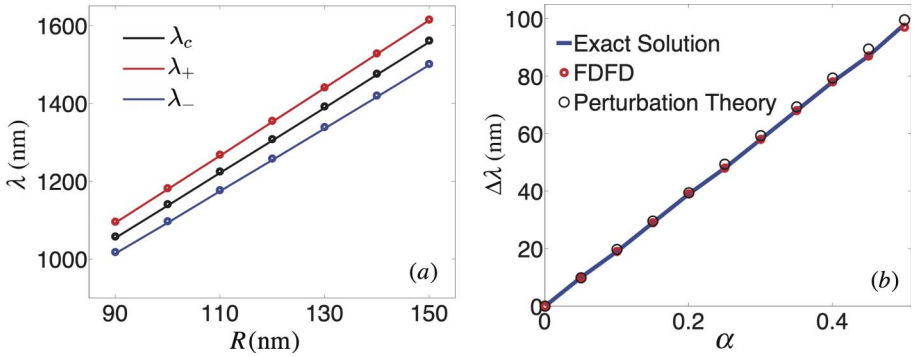

Fig. 2. (a) Resonant wavelength of the cylindrical resonator when the MDM waveguide is absent ($d = \infty$ in Fig. 1) as a function of the radius R of the cavity. The metal is silver, and the MO material is bismuth iron garnet (BIG). The resonant wavelength λ_c without MO activity ($\alpha = 0$) calculated with FDFD is shown with black circles. The resonant wavelengths λ_+ and λ_- when MO activity is present ($\alpha = 0.5$), calculated with FDFD are shown with red and blue circles, respectively. The resonant wavelengths of the cylindrical resonator when the MDM waveguide is absent calculated by solving Eq. (2) are shown with black, red, and blue solid lines. (b) The difference $\Delta\lambda = \lambda_+ - \lambda_-$ between the resonant wavelengths λ_+ and λ_- of the cylindrical resonator when the MDM waveguide is absent ($d = \infty$ in Fig. 1) as a function of the strength of MO activity α calculated with FDFD (red dots) for $R = 120$ nm. Also shown are the exact results calculated by solving Eq. (2) (solid line) and the perturbation theory results [Eq. (3)] (open circles) for the cylindrical resonator when the MDM waveguide is absent.

We note that the assumption $\frac{\alpha}{\epsilon_r} \ll 1$ was used to derive Eq. (3). Figure 2(b) shows the calculated $\Delta\lambda$ as a function of α. We observe that the perturbation theory results [Eq. (3)] for the wavelength splitting $\Delta\lambda$ when MO activity is present and the MDM waveguide is absent agree well with the exact results obtained by solving Eq. (2), confirming the validity of the perturbation theory in describing the properties of the structure. We also observe that for large α the results obtained with the perturbation theory slightly deviate from the exact results, since $\frac{\alpha}{\epsilon_r} \ll 1$ no longer holds.

2.2. Effect of MO activity on the cavity modes

We now consider how the off-diagonal elements in the dielectric permittivity tensor of the MO material [Eq. (1)] affect the cavity modes. The H_z and E_ρ field components inside the cavity can be written as follows:

$$H_z = AJ_m(k_1\rho)e^{im\phi}, \tag{4}$$

$$E_\rho = \frac{1}{\rho\omega\epsilon_0\epsilon_r\epsilon_e}\left(\alpha\rho\frac{\partial H_z}{\partial\rho} - i\epsilon_r\frac{\partial H_z}{\partial\phi}\right) = \frac{A}{\rho\omega\epsilon_0\epsilon_r\epsilon_e}[\alpha k_1\rho J_m'(k_1\rho) + m\epsilon_r J_m(k_1\rho)]e^{im\phi}. \tag{5}$$

Using Eqs. (4) and (5), the $\hat{\phi}$ component of the Poynting vector inside the cavity can be calculated as follows:

$$S_\phi = -\mathrm{Re}\left(\frac{1}{2}E_\rho H_z^*\right) = \mathrm{Re}\left\{-\frac{|A|^2 J_m^*(k_1\rho)}{2\rho\omega\epsilon_0\epsilon_e\epsilon_r}[m\epsilon_r J_m(k_1\rho) + \alpha k_1\rho J_m'(k_1\rho)]\right\}. \tag{6}$$

Based on Eq. (6), without MO activity ($\alpha = 0$), the $\hat{\phi}$ component of the Poynting vector S_ϕ is an odd function of the azimuthal mode number m. The $\hat{\phi}$ component of the total Poynting vector at the resonant wavelength λ_c, which is the sum of the $\hat{\phi}$ components of the Poynting vectors of the $+m$ and $-m$ modes, is therefore zero. Thus, without MO activity, the resonant fields of the cavity are standing waves. On the other hand, when MO activity is present ($\alpha \neq 0$), the $\hat{\phi}$ component of the Poynting vector S_ϕ is no longer an odd function of the mode number m because of the second term in Eq. (6). In addition, the $\pm m$ modes are no longer degenerate. Thus, when $\alpha \neq 0$, the $\hat{\phi}$ component of the total Poynting vector is not zero. Consequently, when MO activity is present, the fields inside the cavity are no longer standing waves, and the cavity becomes a traveling wave resonator.

2.3. Effect of the MDM waveguide on the cavity modes

So far, we investigated the modes of the cylindrical cavity when the MDM waveguide is absent. We demonstrated that, when $\alpha \neq 0$, the cavity mode splits into two modes with resonant wavelengths that can be calculated using Eq. (2). In addition, we showed that MO activity converts the fields of the cavity from standing waves to traveling waves. The resonant wavelengths of the structure of Fig. 1 are affected when the cavity is placed in close proximity to the MDM waveguide. We will first investigate the coupling between the MDM waveguide and the cavity and its effect on the resonant wavelengths of the modes of the structure without MO activity. We will next investigate the effect of the waveguide when MO activity is present.

To investigate the effect of the coupling between the waveguide and the cavity on the resonant wavelengths of the structure, we calculate the transmission, reflection, and absorption spectra without MO activity ($\alpha = 0$) for the structure of Fig. 1. Results are shown in Fig. 3 for different values of the distance d between the cavity and the waveguide. We observe that the MDM waveguide leads to a second resonance in the response

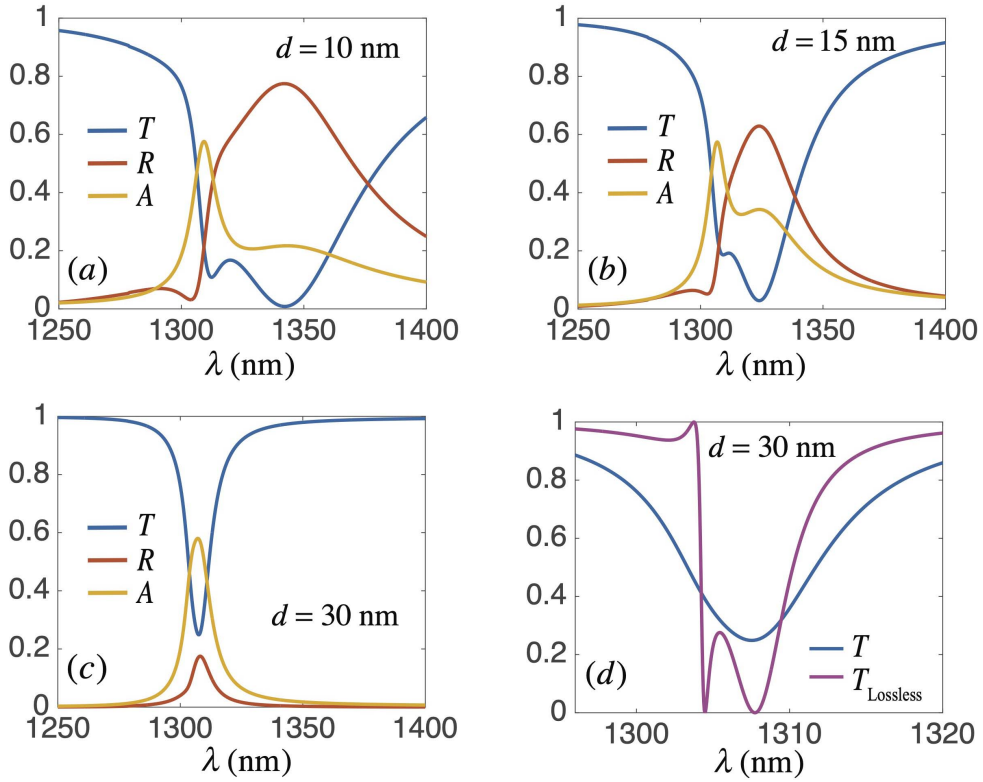

Fig. 3. (a) Transmission T, reflection R, and absorption A spectra without MO activity ($\alpha = 0$) for the structure of Fig. 1 calculated with FDFD for $R = 120$ nm, $W = 50$ nm, and $d = 10$ nm. (b) Same as (a) except $d = 15$ nm. (c) Same as (a) except $d = 30$ nm. (d) Transmission T spectra for $\alpha = 0$ and $d = 30$ nm. Also shown are the transmission spectra in the absence of loss in the metal ($\gamma = 0$).

of the structure [Figs. 3(a) and 3(b)]. Similar to the case where MO activity is present, the two resonant wavelengths are denoted as λ_+ and λ_-. We also observe that decreasing d shifts λ_+ towards longer wavelengths and increases the splitting between the two modes. On the other hand, increasing the distance d, as expected, reduces the effect of the MDM waveguide and brings the resonant wavelengths closer to the resonant wavelengths of the cavity when the MDM waveguide is absent. Figure 3(c) shows the transmission, reflection, and absorption spectra of the structure of Fig. 1 with $d = 30$ nm. We observe that the structure appears to have only one resonant mode. One could conclude that increasing d reduces the effect of the waveguide to the extent that the two modes coincide. However, in order to demonstrate the effect of loss, we show the transmission spectra of the same structure ($d = 30$ nm) in the absence of loss in Fig. 3(d). We observe that in the lossless case the presence of the MDM waveguide leads to a second resonance in the response of the structure. The reason why the second resonance is not observed in the lossy structure [Fig. 3(c)] is that the presence of loss in the system increases the bandwidth of the modes as well as the transmitted power at the resonant wavelengths. As a result, if d is large enough, the two modes become indistinguishable. One can therefore conclude that the waveguide in the proximity of the cavity leads to a new resonant mode, which causes the structure to resonate at two different wavelengths. The appearance of the new resonant mode is due to the geometrical asymmetry in the structure caused by the existence of the waveguide. In the absence of the waveguide, the structure has spatial rotational symmetry. However, the presence of the waveguide breaks the symmetry of the structure and causes the cavity modes to have different resonant wavelengths. One can compare the geometrical asymmetry here to a similar structure with a rectangular resonator, where the difference between the width and the length of the resonator results in different resonant wavelengths for the cavity modes. In addition, we observe that the reflection and absorption at the two resonance wavelengths are different [Figs. 3(a) and 3(b)], with the incident power being mostly absorbed (reflected) at λ_- (λ_+). This difference is due to the fact that the proximity of the waveguide to the cavity affects the effective refractive index experienced by light, which in turn introduces a resonant wavelength at λ_+, at which light is mostly reflected. On the other hand, at $\lambda = \lambda_-$, the drop in transmission is mostly due to absorption. In addition, the resonant wavelength λ_- is almost independent of d, whereas the resonant wavelength λ_+ is strongly dependent on d. When the MDM waveguide is absent, any line through the center of the cylindrical cavity is an axis of symmetry. However, in the presence of the waveguide, this no longer holds. The MDM waveguide breaks the symmetry with respect to the x axis. On the other hand, the structure is still symmetric with respect to the y axis. As a result, only one mode, the mode at $\lambda = \lambda_+$, is affected. The analogy between rectangular resonators can be used again to

explain the physics behind this phenomenon. The effect of decreasing the distance between the cavity and the waveguide is similar to changing the length of a rectangular resonator while keeping its width constant.

We next investigate the effect of MO activity on the performance of the device. As discussed above, the cavity mode without MO activity splits into two modes when MO activity is present. The MDM waveguide also leads to splitting of the modes of the structure by breaking its geometrical symmetry. Here, we investigate the performance of the device in the presence of both the MDM waveguide and MO activity. In this case, the mode splitting is due to both geometrical asymmetry and MO activity. As discussed above, when d is large enough ($d > 20$ nm), the presence of loss makes the wavelength splitting due to the MDM waveguide unobservable. Therefore, here, in order to analyze the effect of the MDM waveguide when MO activity is present on the wavelength splitting $\Delta\lambda$, the metal (silver) is assumed to be lossless. It should be noted that including the effect of loss does not significantly change the value of the calculated $\Delta\lambda$. However, in the presence of loss, the splitting becomes unobservable for large d. Figure 4 shows the wavelength splitting $\Delta\lambda$ as a function of d for different strengths of MO activity ($\alpha = 0$, 0.05, 0.1, 0.15, 0.2) and for lossless metal ($\gamma = 0$). We observe that, as expected, decreasing d increases the splitting $\Delta\lambda$. In addition, as d increases, the effect of the MDM waveguide becomes less significant, and the wavelength splitting is mostly due to the presence of MO activity. Thus, as d increases, the wavelength splitting $\Delta\lambda$ approaches the value corresponding to the absence of the waveguide calculated by solving Eq. (2) (Fig. 4).

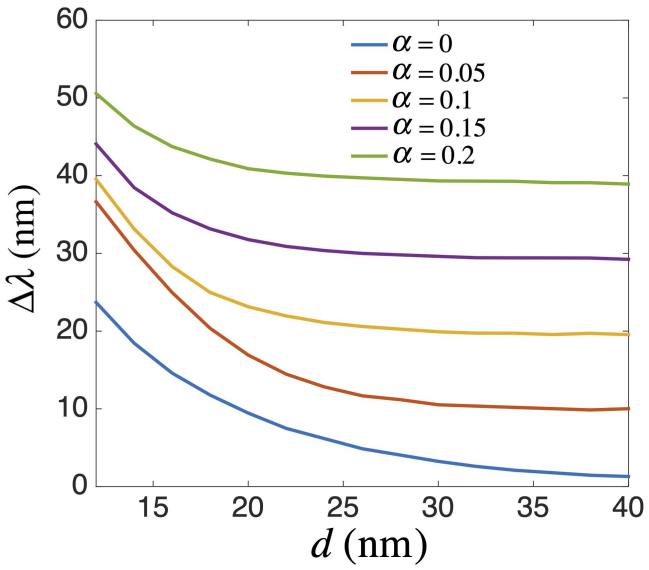

Fig. 4. Difference $\Delta\lambda = \lambda_+ - \lambda_-$ between the resonant wavelengths λ_+ and λ_- of the structure shown in Fig. 1 with $W = 50$ nm and $R = 120$ nm as a function of the distance d between the cavity and the waveguide. Results are shown for different strengths of MO activity ($\alpha = 0$, 0.05, 0.1, 0.15, 0.2) and for lossless metal ($\gamma = 0$).

2.4. Design of a nanoplasmonic isolator

After investigating the cavity in the absence and presence of the MDM waveguide and MO activity, we propose an all-optical isolator based on the structure shown in the schematic of Fig. 1. As discussed above, the presence of the MDM waveguide and MO activity leads to mode splitting. In addition, the resonant cavity fields when MO activity is present become traveling waves. Traveling wave modes do not decay equally into the forward and backward propagating MDM waveguide modes due to momentum matching[43]. The unequal decay rates and the frequency splitting enable the device to operate as an isolator. Figures 5(a)–5(c) show the transmission, reflection, and absorption spectra, respectively, for a structure with $R = 120$ nm, $d = 15$ nm, and $W = 50$ nm in the presence (blue and red curves) and absence (black curve) of MO activity. The blue and red curves in Fig. 5(a) show the transmission spectra when MO activity is present, and light is incident from the left and right directions, respectively. Compared to the case where there is no MO activity (black curve), the presence of MO activity shifts the resonant wavelengths λ_- and λ_+ towards shorter and longer wavelengths, respectively. In addition, we observe that, when MO activity is present, the resonant mode at $\lambda = \lambda_- = 1310$ nm is not excited when light is incident from the right direction (red curve). On the other hand, the resonant mode at $\lambda = \lambda_+$ is excited in both cases with a small difference in the value of the transmission depending on whether light is incident from the left (blue curve) or right (red curve) direction [Fig. 5(a)]. The small difference in transmission for modes incident from different directions at $\lambda = \lambda_+$ is due to the difference in absorption [Fig. 5(c)]. As mentioned above, the presence of MO activity converts the fields of the structure from standing waves to traveling waves. Since traveling wave cavities exhibit different decay behavior into the forward and backward propagating waveguide modes, the transmission spectra depend on the direction of the incident MDM waveguide mode. As shown in Fig. 5(b), when MO activity is present, the reflection spectra of the structure for light incident from the left (blue curve) and right (red curve) directions are identical. However, the absorption spectra when MO activity is present [Fig. 5(c)] depend on whether light is incident from the left (blue curve) or right (red curve) direction. The difference in the transmission spectra when MO activity is present for light incident from the left and right directions is due to this difference in the absorption spectra. We also observe that at $\lambda = \lambda_- = 1310$ nm when MO activity is present, if light is incident from the left (blue curve), it is mostly absorbed [Fig. 5(c)], whereas, if light is incident from the right (red curve), it is mostly transmitted [Fig. 5(a)]. The proposed structure therefore operates as an optical isolator at $\lambda = \lambda_- = 1310$ nm in the presence of a static magnetic field. Figure 5(d) shows the magnetic field profile at $\lambda = \lambda_- = 1310$ nm when light is incident from the left (bottom) and right (top) directions, confirming that the device operates as an isolator when MO activity is present.

We next investigate in detail the effect of the geometrical parameters of the structure on its performance. As mentioned

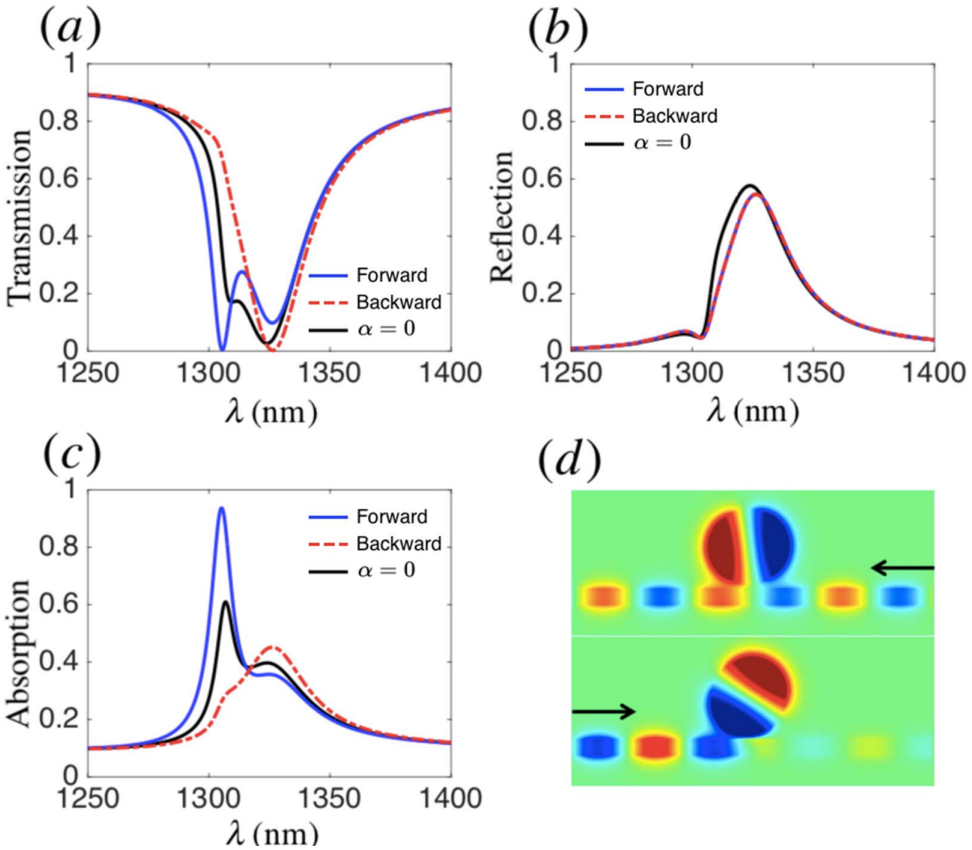

Fig. 5. (a) Transmission spectra for the structure of Fig. 1 calculated with FDFD for $R = 120$ nm, $d = 15$ nm, and $W = 50$ nm, when MO activity is present ($\alpha = 0.06$), and light is incident from the left (forward) and right (backward) directions. Also shown are the transmission spectra without MO activity ($\alpha = 0$). (b) Reflection spectra for the structure of Fig. 1. All other parameters are as in (a). (c) Absorption spectra for the structure of Fig. 1. All other parameters are as in (a). (d) Magnetic field profiles at $\lambda = \lambda_{-}$=1310 nm when MO activity is present ($\alpha = 0.06$), and light is incident from the left (bottom figure) and right (top figure) directions. All other parameters are as in (a).

above, the structure is used as an optical isolator at the resonant wavelength λ_{-} when MO activity is present. The resonant wavelength λ_{-} is itself a function of the parameters of the structure. In Fig. 6(a), we show the resonant wavelength λ_{-} as a function of the radius R of the cylindrical cavity and the distance d between the cavity and the waveguide (Fig. 1). As also discussed above, the resonant wavelength λ_{-} increases approximately linearly with the radius R of the cylindrical cavity. In addition, the

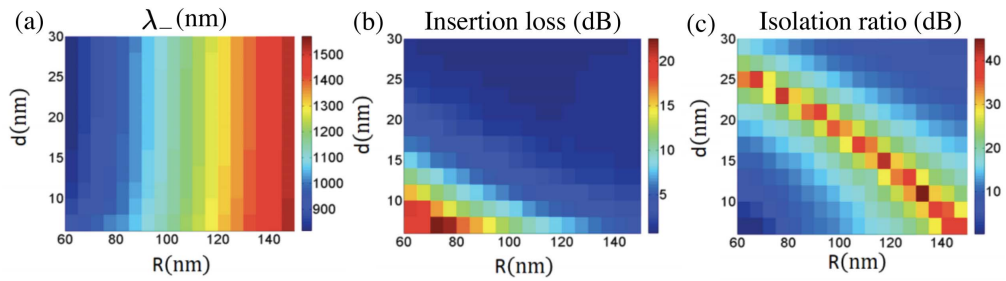

Fig. 6. (a) Resonant wavelength λ_{-} when MO activity is present for the structure of Fig. 1 as a function of the radius R of the cylindrical cavity and the distance d between the cavity and the waveguide calculated with FDFD. All other parameters are as in Fig. 5(a). (b) Insertion loss, defined as $-10\log_{10}(T_{on})$, for the structure of Fig. 1 as a function of R and d calculated with FDFD. Here, T_{on} is the transmission for light incident from the right direction. The insertion loss is calculated at the resonant wavelength λ_{-} when MO activity is present, which is a function of R and d. (c) Isolation ratio for the structure of Fig. 1 as a function of R and d calculated with FDFD. The isolation ratio is defined as the ratio of the transmission for light incident from the right direction T_{on} to the transmission for light incident from the left direction T_{off}. The isolation ratio is calculated at the resonant wavelength λ_{-} when MO activity is present, which is a function of R and d.

presence of the MDM waveguide shifts the cavity resonance towards longer wavelengths, and the resonant wavelength λ_- increases as d decreases [Fig. 6(a)]. Thus, the wavelength of operation of the isolator can be tuned by adjusting the geometrical parameters of the structure. In Fig. 6(b), we show the insertion loss of the isolator, defined as $-10\log_{10}(T_{on})$, as a function of R and d. Here, T_{on} is the transmission for light incident from the right direction. The insertion loss is calculated at the resonant wavelength λ_- when MO activity is present, which, as mentioned above, is a function of R and d [$\lambda_- = \lambda_-(R,d)$]. We observe that increasing d decreases the insertion loss. This is expected, since increasing d decreases the coupling between the MDM waveguide and the cavity[43] so that more power is transmitted on resonance. Finally, in Fig. 6(c), we show the isolation ratio of the structure, defined as the ratio of the transmission for light incident from the right direction T_{on} to the transmission for light incident from the left direction T_{off} [Fig. 5(d)]. Similar to the insertion loss, the isolation ratio is also calculated at the resonant wavelength $\lambda_-(R,d)$ when MO activity is present. We observe that for a given R the isolation ratio is maximized for a specific value of d. Further increasing the distance d decreases the insertion loss but also decreases the isolation ratio. In other words, there is a tradeoff between the isolation ratio and the insertion loss, as the geometrical parameters of the structure are varied.

3. Conclusions

We introduced a nanoplasmonic isolator, which consists of a cylindrical resonator placed close to an MDM waveguide. The waveguide and resonator are filled with an MO material, and the structure is under a static magnetic field. We found that, in the absence of the MDM waveguide, the cavity mode without MO activity splits into two modes when MO activity is present. We also found that the MDM waveguide leads to a second resonance in the response of the structure, due to the geometrical asymmetry caused by the waveguide. In the presence of MO activity, the mode splitting is due to both geometrical asymmetry and MO activity. In addition, when MO activity is present, the cavity becomes a traveling wave resonator with unequal decay rates into the forward and backward propagating MDM waveguide modes. As a result, the transmission of the structure depends on the direction of the incident light. When light is incident from one direction, it is mostly absorbed, whereas, when it is incident from the other direction, it is mostly transmitted. The proposed structure therefore operates as an optical isolator. We finally showed that there is a tradeoff between the isolation ratio and the insertion loss of the proposed isolator.

References

1. D. Jalas, A. Petrov, M. Eich, W. Freude, S. Fan, Z. Yu, R. Baets, M. Popović, A. Melloni, J. D. Joannopoulos, M. Vanwolleghem, C. R. Doerr, and H. Renner, "What is—and what is not—an optical isolator," Nat. Photon. **7**, 579 (2013).
2. Z. Yu, G. Veronis, Z. Wang, and S. Fan, "One-way electromagnetic waveguide formed at the interface between a plasmonic metal under a static magnetic field and a photonic crystal," Phys. Rev. Lett. **100**, 023902 (2008).
3. K. Fang, Z. Yu, and S. Fan, "Photonic Aharonov–Bohm effect based on dynamic modulation," Phys. Rev. Lett. **108**, 153901 (2012).
4. S. Yu, X. Piao, S. Koo, J. H. Shin, S. H. Lee, B. Min, and N. Park, "Mode junction photonics with a symmetry-breaking arrangement of mode-orthogonal heterostructures," Opt. Express **19**, 25500 (2011).
5. A. E. Miroshnichenko, E. Brasselet, and Y. S. Kivshar, "Reversible optical nonreciprocity in periodic structures with liquid crystals," Appl. Phys. Lett. **96**, 063302 (2010).
6. H. Lira, Z. Yu, S. Fan, and M. Lipson, "Electrically driven nonreciprocity induced by interband photonic transition on a silicon chip," Phys. Rev. Lett. **109**, 033901 (2012).
7. Z. Yu, Z. Wang, and S. Fan, "One-way total reflection with one-dimensional magneto-optical photonic crystals," Appl. Phys. Lett. **90**, 121133 (2007).
8. N. Sugimoto, T. Shintaku, A. Tate, H. Terui, M. Shimokozono, E. Kubota, M. Ishii, and Y. Inoue, "Waveguide polarization-independent optical circulator," IEEE Photon. Technol. Lett. **11**, 355 (1999).
9. R. Takei and T. Mizumoto, "Design and simulation of silicon waveguide optical circulator employing nonreciprocal phase shift," Jpn. J. Appl. Phys. **49**, 052203 (2010).
10. L. Bi, J. Hu, P. Jiang, D. H. Kim, G. F. Dionne, L. C. Kimerling, and C. A. Ross, "On-chip optical isolation in monolithically integrated non-reciprocal optical resonators," Nat. Photon. **5**, 758 (2011).
11. Z. Wang and S. Fan, "Optical circulators in two-dimensional magneto-optical photonic crystals," Opt. Lett. **30**, 1989 (2005).
12. Y. Wang, D. Zhang, S. Xu, Z. Ouyang, and J. Li, "Low-loss Y-junction two-dimensional magneto-photonic crystals circulator using a ferrite cylinder," Opt. Commun. **369**, 1 (2016).
13. W. L. Barnes, A. Dereux, and T. W. Ebbesen, "Surface plasmon subwavelength optics," Nature **424**, 824 (2003).
14. S. A. Maier, *Plasmonics: Fundamentals and Applications* (Springer, 2007).
15. A. R. Davoyan and N. Engheta, "Nanoscale plasmonic circulator," New J. Phys. **15**, 083054 (2013).
16. D. Regatos, D. Fariña, A. Calle, A. Cebollada, B. Sepúlveda, G. Armelles, and L. M. Lechuga, "Au/Fe/Au multilayer transducers for magneto-optic surface plasmon resonance sensing," J. Appl. Phys. **108**, 054502 (2010).
17. B. Sepúlveda, L. M. Lechuga, and G. Armelles, "Magnetooptic effects in surface-plasmon-polaritons slab waveguides," J. Light. Technol. **24**, 945 (2006).
18. X. Luo, M. Zhou, J. Liu, T. Qiu, and Z. Yu, "Magneto-optical metamaterials with extraordinarily strong magneto-optical effect," Appl. Phys. Lett. **108**, 131104 (2016).
19. V. I. Belotelov, L. L. Doskolovich, and A. K. Zvezdin, "Extraordinary magneto-optical effects and transmission through metal-dielectric plasmonic systems," Phys. Rev. Lett. **98**, 077401 (2007).
20. B. Sepúlveda, J. B. González-Díaz, A. García-Martín, L. M. Lechuga, and G. Armelles, "Plasmon-induced magneto-optical activity in nanosized gold disks," Phys. Rev. Lett. **104**, 147401 (2010).
21. M. I. Abdelrahman and F. Monticone, "Broadband and giant nonreciprocity at the subwavelength scale in magnetoplasmonic materials," Phys. Rev. B **102**, 155420 (2020).
22. A. López-Ortega, M. Zapata-Herrera, N. Maccaferri, M. Pancaldi, M. Garcia, A. Chuvilin, and P. Vavassori, "Enhanced magnetic modulation of light polarization exploiting hybridization with multipolar dark plasmons in magnetoplasmonic nanocavities," Light. Sci. Appl. **9**, 1 (2020).
23. Ş. E. Kocabaş, G. Veronis, D. A. B. Miller, and S. Fan, "Modal analysis and coupling in metal-insulator-metal waveguides," Phys. Rev. B **79**, 035120 (2009).
24. Z. Han, E. Forsberg, and S. He, "Surface plasmon gratings formed in metal-insulator-metal waveguides," IEEE Photon. Technol. Lett. **19**, 91 (2007).
25. V. F. Nezhad, S. Abaslou, and M. S. Abrishamian, "Plasmonic band-stop filter with asymmetric rectangular ring for WDM networks," J. Opt. **15**, 055007 (2013).
26. Z. Han, L. Liu, and E. Forsberg, "Ultra-compact directional couplers and Mach–Zehnder interferometers employing surface plasmon polaritons," Opt. Commun. **259**, 690 (2006).
27. Q. Zhang, X.-G. Huang, X.-S. Lin, J. Tao, and X.-P. Jin, "A subwavelength coupler-type MIM optical filter," Opt. Express **17**, 7549 (2009).

28. A. Dolatabady, N. Granpayeh, and V. F. Nezhad, "A nanoscale refractive index sensor in two dimensional plasmonic waveguide with nanodisk resonator," Opt. Commun. **300**, 265 (2013).
29. K. Wen, Y. Hu, L. Chen, J. Zhou, L. Lei, and Z. Guo, "Fano resonance with ultra-high figure of merits based on plasmonic metal-insulator-metal waveguide," Plasmonics **10**, 27 (2015).
30. Y. Huang, C. Min, P. Dastmalchi, and G. Veronis, "Slow-light enhanced subwavelength plasmonic waveguide refractive index sensors," Opt. Express **23**, 14922 (2015).
31. H. Lu, X. Liu, L. Wang, Y. Gong, and D. Mao, "Ultrafast all-optical switching in nanoplasmonic waveguide with Kerr nonlinear resonator," Opt. Express **19**, 2910 (2011).
32. Z. Yu, G. Veronis, S. Fan, and M. L. Brongersma, "Gain-induced switching in metal-dielectric-metal plasmonic waveguides," Appl. Phys. Lett. **92**, 041117 (2008).
33. C. Min and G. Veronis, "Absorption switches in metal-dielectric-metal plasmonic waveguides," Opt. Express **17**, 10757 (2009).
34. A. Haddadpour, V. F. Nezhad, Z. Yu, and G. Veronis, "Highly compact magneto-optical switches for metal-dielectric-metal plasmonic waveguides," Opt. Lett. **41**, 4340 (2016).
35. J.-S. Pae, S.-J. Im, K.-S. Ho, C.-S. Ri, S.-B. Ro, and J. Herrmann, "Ultracompact high-contrast magneto-optical disk resonator side-coupled to a plasmonic waveguide and switchable by an external magnetic field," Phys. Rev. B **98**, 041406 (2018).
36. Y. Xu, X. Wang, H. Deng, and K. Guo, "Tunable all-optical plasmonic rectifier in nanoscale metal–insulator–metal waveguides," Opt. Lett. **39**, 5846 (2014).
37. H. Lu, X. Liu, D. Mao, L. Wang, and Y. Gong, "Tunable band-pass plasmonic waveguide filters with nanodisk resonators," Opt. Express **18**, 17922 (2010).
38. T. Tepper and C. A. Ross, "Pulsed laser deposition and refractive index measurement of fully substituted bismuth iron garnet films," J. Cryst. Growth **255**, 324 (2003).
39. M. N. Deeter, S. M. Bon, G. W. Day, G. Diercks, and S. Samuelson, "Novel bulk iron garnets for magneto-optic magnetic field sensing," IEEE Trans. Magn. **30**, 4464 (1994).
40. K. Liu, A. Torki, and S. He, "One-way surface magnetoplasmon cavity and its application for nonreciprocal devices," Opt. Lett. **41**, 800 (2016).
41. P. Zeeman, "The effect of magnetisation on the nature of light emitted by a substance," Nature **55**, 347 (1897).
42. J. Wang, K. H. Fung, H. Y. Dong, and N. X. Fang, "Zeeman splitting of photonic angular momentum states in a gyromagnetic cylinder," Phys. Rev. B **84**, 235122 (2011).
43. Q. Li, T. Wang, Y. Su, M. Yan, and M. Qiu, "Coupled mode theory analysis of mode-splitting in coupled cavity system," Opt. Express **18**, 8367 (2010).